Mesoscale Dynamics of the Near-Dryline Environment: Analysis of Data from COPS-91

HOWARD B. BLUESTEIN AND TODD M. CRAWFORD

School of Meteorology, University of Oklahoma, Norman, Oklahoma

(Manuscript received 16 April 1996, in final form 10 December 1996)

ABSTRACT

A technique is introduced using surface data from triangular networks of adjacent mesonet stations to estimate the terms in the horizontal equation of motion at anemometer level (10 m) on either side of the dryline in the southern plains of the United States. Data from an instrumented surface mesonetwork in the Texas panhandle and western and central Oklahoma during the Cooperative Oklahoma Profiler Studies (COPS-91) field program were employed for this purpose. East of the dryline and surface pressure trough the vertical-mixing term had a component normal and to the right of the surface wind in accord with Ekman theory; west of the dryline and surface pressure trough the vertical-mixing term had a component normal and to the left of the surface wind in disagreement with Ekman theory. It is suggested that disagreements with Ekman theory may be due to baroclinic effects in the boundary layer. It is also shown that during the day both the westward component of the pressure gradient force and the easterly component of the surface wind increased east of the dryline, in accord with the ''inland sea breeze'' hypothesis, and that the maximum easterly wind component usually lagged the maximum westward component of the pressure gradient force by several hours.

1. Introduction

It may be inferred from observational and numerical studies that a knowledge of boundary layer dynamics along and near the dryline is essential for our understanding of dryline behavior (Schaefer 1974a,b; McCarthy and Koch 1982; Sun and Wu 1992; Ziegler et al. 1995) and convection initiation (Rhea 1966; Koch and McCarthy 1982; Parsons et al. 1991; Hane et al. 1997). In particular, the vertical mixing of momentum and water vapor and the east–west variation in the depth of the moist boundary layer have been shown to play important roles in the behavior of the dryline.

Since the dryline exhibits significant variability on subsynoptic scales, it is difficult to study using data from the standard observing network alone. To study the dryline properly, nonstandard instrumentation and/or platforms capable of making measurements on the mesoscale and convective scale, such as aircraft, special or mobile soundings, and surface mesonetworks, are required. Crawford and Bluestein (1997) presented analyses of data collected during the Cooperative Oklahoma Profiler Studies field program in May 1991 (COPS-91) (Hane et al. 1993), from which the characteristics of dryline passage were discussed. Differences between eastward- and westward-moving drylines were highlighted. The purpose of this paper is to use COPS-91 data to test hypotheses for the mesoscale dynamics of the dryline *environment* that have been proposed on the basis of numerical simulations.

We will focus on the following problems.

1) How is the vertical mixing of momentum near the dryline, both during the day and at night, related to the other physical effects in the equation of motion such as the pressure gradient force and the Coriolis force?
2) Is the ''inland sea breeze'' hypothesis (Ogura and Chen 1977; Sun and Ogura 1979; Sun and Wu 1992) consistent with the observations? According to the inland sea breeze hypothesis, a vertical circulation may be excited normal to the dryline if a strong virtual temperature gradient, comparable in magnitude to that typically observed along the sea-breeze front in coastal regions, is produced across it near the ground as a result of a diurnal variation in nonuniform surface heating.

In section 2 we discuss the nature of the data and the processing techniques we used. A method for estimating the terms in the horizontal equation of motion using filtered, mesoscale surface data from triangular networks of adjacent mesonet stations is introduced in section 3. Section 4 contains analyses and a discussion of the different forces east and west of the dryline as a function of the time of day. A summary of the results of our study, conclusions, and suggestions for continued work are found in section 5.

Corresponding author address: Dr. Howard B. Bluestein, School of Meteorology, University of Oklahoma, 100 E. Boyd, Rm. 1310, Norman, OK 73019.
E-mail: hblue@ou.edu

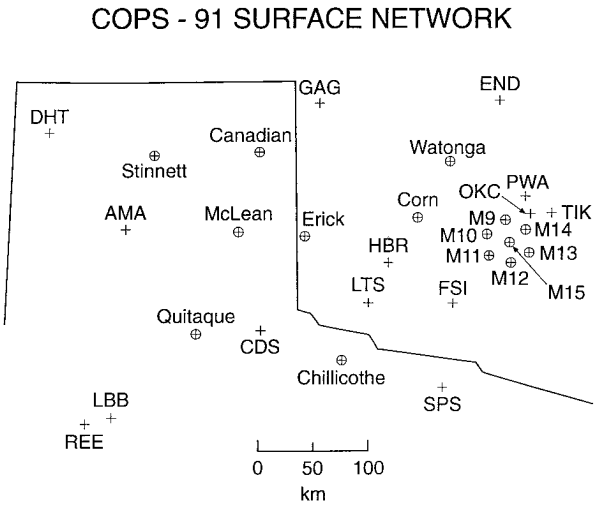

FIG. 1. Distribution of surface observing sites during COPS-91. PAM-II sites are represented by circles with inscribed crosses; standard hourly surface observing sites are represented by crosses.

2. Data and data processing

The data and data processing procedures are discussed in Crawford and Bluestein (1997). We repeat them here to aid the reader. The network of surface observing sites during COPS-91 is shown in Fig. 1. Eight sites of the 15 PAM-II (Portable Automated Mesonetwork) (Brock et al. 1986) stations from the National Center for Atmospheric Research (NCAR) were chosen to fill in the gaps between neighboring standard hourly surface observation sites; seven stations were located in a finer-scale grid in central Oklahoma for other studies. At each site, 60-s averages of station pressure, dry-bulb temperature, relative humidity, water vapor mixing ratio, and the zonal (u) and meridional (v) components of the wind were available every 60 s. Calculations of monthly averages of each variable were used to determine and remove biases subjectively and to discard apparently erroneous data. It was not necessary to correct for obstructing trees and buildings (Fujita and Wakimoto 1982) at most sites in the Texas panhandle and western Oklahoma because nearly all were located in completely open space devoid of buildings, trees, fences, etc. (C. Hane 1996, personal communication); the site at Stinnett, however, was situated approximately 30 m away from a water tower to its northeast. However, since the wind direction was most often from the west or southwest in the cases cited in this study, the obstacle was most frequently downstream from the station and hence blockage should not have been a significant factor. Missing data were estimated through temporal linear interpolation. Overall, 6.3% of all the PAM-II data were missing. Of these, most occurred at Quitaque, where approximately two-thirds of the data (representing approximately 20 days) were not available, and at McLean, where approximately one-third of the data were missing. In the few instances in which interpolated data were used, the longest time interval over which data were interpolated was less than 1 h.

Two of the National Severe Storms Laboratory's (NSSL) mobile laboratories were equipped with with the Cross-chain Loran Atmospheric Sounding System (CLASS) (Rust et al. 1990). Soundings were available at locations both west and east of the dryline at various times, and in situ aircraft measurements made by the NOAA P-3 (Hane et al. 1993) were used in two cases.

3. Technique for analysis of the terms in the equation of motion

The mesoscale dynamics of the near-dryline environment may be analyzed by considering the temporal variation in the forces represented in the horizontal equation of motion and their relative magnitudes and directions with respect to each other. The vector form of the horizontal equation of motion at the ground, with height above mean sea level (MSL) (z) as the vertical coordinate, may be expressed as

$$\frac{\partial \mathbf{v}}{\partial t} + (\mathbf{v}\cdot\nabla)\mathbf{v} + w\frac{\partial \mathbf{v}}{\partial z} = -f\mathbf{k}\times\mathbf{v} - \frac{1}{\rho}\nabla p + \mathbf{F}_H + \mathbf{F}_Z, \quad (1)$$

where $\mathbf{v}$ is the horizontal wind vector, w is the vertical velocity, f is the Coriolis parameter, $\mathbf{k}$ is the unit vector pointing upward, ρ is the density, p is the pressure, $\mathbf{F}_H$ is the acceleration due to turbulent horizontal mixing of horizontal momentum, and $\mathbf{F}_Z$ is the acceleration due to turbulent vertical mixing of horizontal momentum. Equation (1) neglects the relatively small terms that contain the effects of the curvature of the earth. The turbulent mixing terms, with density variations neglected, may be expressed as

$$\mathbf{F}_H = -\left\{\left[\frac{\partial(\overline{u'^2})}{\partial x} + \frac{\partial(\overline{u'v'})}{\partial y}\right]\mathbf{i} + \left[\frac{\partial(\overline{v'u'})}{\partial x} + \frac{\partial(\overline{v'^2})}{\partial y}\right]\mathbf{j}\right\} \quad (2)$$

$$\mathbf{F}_Z = -\left\{\left[\frac{\partial(\overline{u'w'})}{\partial z}\right]\mathbf{i} + \left[\frac{\partial(\overline{v'w'})}{\partial z}\right]\mathbf{j}\right\}, \quad (3)$$

where the primed terms represent eddy values; the overbarred terms represent mean values; and $\mathbf{i}$ and $\mathbf{j}$ are the unit vectors directed toward the east and north, respectively.

The vertical-mixing term may be further subdivided into a part representing barotropic and baroclinic processes (Bell and Bosart 1988). A portion of the barotropic part of the vertical-mixing term can be approximated as the stress resulting from surface drag ($\mathbf{F}_D$) associated with approximately unidirectional shear below anemometer level, while the other part results from

the change in wind direction with height associated with the Ekman turning of the wind shear vector with height above anemometer level. The combined effect of the latter and the baroclinic part is represented by the stress associated with the vertical divergence of the vertical gradient of the horizontal velocity ($\mathbf{F}_A$):

$$\mathbf{F}_Z = \mathbf{F}_D + \mathbf{F}_A. \tag{4}$$

In other words, $\mathbf{F}_A$ represents that portion of the vertical-mixing term that results from the change in the direction of the vertical wind shear vector with height, while $\mathbf{F}_D$ represents that portion of the vertical-mixing term that results from the change in wind shear vector with height due to surface drag only.

The surface drag term may be parameterized in terms of the anemometer-level wind ($\mathbf{v}_o$), a drag coefficient (C_D), and the approximate boundary layer depth (1000 m) as follows (Bluestein 1992, 241), when wind shear away from the ground is negligible (Bell and Bosart 1988):

$$\mathbf{F}_D = \frac{1}{1000\ \text{m}}\left(-C_D|\mathbf{v}_o|^2\frac{\mathbf{v}_o}{|\mathbf{v}_o|}\right). \tag{5}$$

Unlike $\mathbf{F}_{D,}$ the barotropic part of $\mathbf{F}_A$ at anemometer level is not necessarily directed in the direction opposite to that of the wind, owing to Ekman turning of the wind with height above anemometer level (Arya 1985). The baroclinic part of the vertical-mixing term is also not necessarily directed in the direction opposite that of the wind at anemometer level, especially when the thermal-wind shear vector changes direction with height. The decomposition of the friction term into $\mathbf{F}_D$ and $\mathbf{F}_A$ is useful if the barotropic part of the stress really goes to zero at the top of the boundary layer, which in this case is assumed to be 1000 m, and if the wind at anemometer level is representative of the mean wind in the boundary layer. Since our technique makes use only of surface data, we must be cautious when applying (4) and (5) to the COPS-91 dataset. Wyngaard (1984) has demonstrated that in a well-mixed boundary layer, the baroclinic part of the stress is due to the entrainment of momentum across the top of the layer. We cannot measure this effect, which could be significant if at the top of the boundary layer there were a relatively large component of temperature gradient normal to the wind. Since we ignore this effect, there is additional uncertainty about errors that may be introduced.

For balanced flow (1) in which $\mathbf{F}_H$ can be neglected, the vertical-mixing term may be expressed as

$$\mathbf{F}_Z = f\mathbf{k} \times (\mathbf{v} - \mathbf{v}_g) = f\mathbf{k} \times \mathbf{v}_a. \tag{6}$$

The total mixing term $\mathbf{F}_Z$ is thus directed normal and to the left of the ageostrophic wind (Arya 1985) in the Northern Hemisphere. For example, if the total wind at anemometer level were westerly, the total mixing term in a balanced, barotropic atmospheric would be directed toward the southwest (Arya 1985; Bannon and Salem 1995; Bluestein 1992, Fig. 4.54 on p. 240) and the ageostrophic wind would be southeasterly. At anemometer level in a balanced, barotropic boundary layer, the vertical mixing term must be directed opposite and to the *right* of the wind. The physical interpretation of the deviation to the right of the vertical mixing term is that net momentum directed to the right of the wind is mixed down as a result of the Ekman profile, which spirals to the right with height. Deviations from the aforementioned behavior call into question the following assumptions made in Ekman theory: whether the flow is balanced, whether baroclinic effects are significant, whether (behind the dryline, where during the day thermals may be intense and act over a deep layer) it is valid to parameterize the stress as proportional to the vertical shear, or whether momentum actually diffuses in the downgradient direction (i. e., whether the proportionality constant is positive).

Two of the three terms on the left-hand side of (1), the local time derivative term and the horizontal advection term, and two on the right-hand side of (1), the Coriolis term and the pressure gradient term, can be calculated from analyses of the mesonet and conventional data. The vertical-advection term is ignored because vertical velocity is assumed to be zero at the ground; it may be significant, however, over the far western portions of the network (Fig. 1), where the elevation increases modestly to the west, if the horizontal wind has an easterly component of 10 m s^{-1} or greater (Bluestein 1992, 301).

In order to reduce the effects of subgrid-scale noise, the 1-min PAM-II mesonet wind and pressure data for the entire month of May were temporally filtered. For an average station separation of 100 km (Fig. 1) and a representative advective speed of 5 m s^{-1}, features having periods shorter than the Nyquist period of 4×10^4 s (approximately 11 h) may be contaminated by aliasing. The temporal filter we used reduced the amplitude of features having periods shorter than 3 h by more than 95%, while retaining 80% or more of the amplitude of features having periods of 12 h or longer. Thus, the filter does not eliminate the features of interest of our study, which have periods of 12 h or greater. A comparison of the filtered time series with the unfiltered time series (not shown) verified the effectiveness of the filter. Our choice of filter represents a compromise necessary to retain data representative of the mesoscale spatial scales of interest of hundreds of kilometers, while avoiding aliasing on the convective scale. A filter having the same response as that applied to the PAM-II data was also applied to wind and pressure data from the standard hourly surface network.

The local time derivative and Coriolis terms were calculated from the temporally filtered wind data linearly interpolated at the centroids of the triangles formed by each group of three neighboring mesonet stations. Triangles that were most like equilateral triangles were chosen to minimize interpolation errors. The horizontal

advection term was computed at the centroids of each triangle; the horizontal derivatives of the components of the wind field were computed from the slope of a plane that was fitted to the filtered wind components (Davies-Jones 1993).

We took into account the slope of terrain by incorporating vertical shear, much of which is probably due to friction, into the calculations (Schaefer 1973) using

$$(\nabla u)_e = (\nabla u)_z + \frac{\partial u}{\partial z}(\nabla E)_z, \tag{7a}$$

$$(\nabla v)_e = (\nabla v)_z + \frac{\partial v}{\partial z}(\nabla E)_z, \tag{7b}$$

where e is the vertical coordinate in a constant-altitude system (in this case e is held fixed at the ground), z is the vertical coordinate in a mean sea level system, and E is the surface elevation (MSL). The terrain slope gradient $(\nabla E)_z$ was computed by fitting a plane to the elevation MSL of each PAM site in each triangle. The elevations of neighboring PAM-II stations differ by about 100–200 m or less. The vertical shear vector $\partial\mathbf{v}/\partial z$ was estimated from the average in the lowest 250 m AGL of seven special CLASS-sounding hodographs on 15 May, a day when there was excellent coverage near the dryline. The average $\partial u/\partial z$ and $\partial v/\partial z$ were 3.5×10^{-3} s^{-1} and -9.5×10^{-3} s^{-1}, respectively. Even though our method of calculating low-level vertical shear does not take into account soundings from every case, the magnitude of the error introduced is at best small compared to the other terms in (7), but at worst just as large as the other terms. For example, under typical conditions,

$$\begin{aligned} |(\nabla E)_z|\left|\frac{\partial \mathbf{v}}{\partial z}\right| &\sim \left(\frac{100\text{ m}}{100\text{ km}}\right)\left(\frac{5\text{–}10\text{ m s}^{-1}}{1000\text{ m}}\right) \\ &\sim 5 \times 10^{-6}\text{ s}^{-1}\text{–}10^{-5}\text{ s}^{-1} \\ &\leq |(\nabla|\mathbf{v}|)_z| \sim \frac{1\text{–}5\text{ m s}^{-1}}{100\text{ km}} \\ &\sim 1\text{–}5 \times 10^{-5}\text{ s}^{-1}. \end{aligned}$$

In this study we *have* taken into account the vertical shear and realize that our calculations of horizontal derivatives of the wind field may at times contain substantial errors. However, it later will be seen that the advective terms in (1) are usually relatively small.

In order to estimate the pressure-gradient term, the temporally filtered station-pressure measurements at each PAM-II mesonet site and the altimeter settings at the standard hourly observing sites were reduced hydrostatically using a standard atmosphere lapse rate, to the average elevation of all the stations (637 m MSL). The greatest difference between the average elevation and the elevation of a PAM-II site is 370 m. The greatest difference between reduced pressure calculated using a standard atmosphere lapse rate and reduced pressure using a dry-adiabatic lapse rate is around 0.5 mb. The pressure gradient, however, could not be estimated accurately by fitting a plane to temporally filtered pressure data at the vertices of triangles of neighboring PAM-II sites, owing to the relatively small spacing between PAM-II sites. For example, to compute accurately a typical pressure gradient on the order of 1 mb per 100 km, the pressure at each site would have to be known to within 0.1 mb, while the rms (root-mean-square) error of the PAM-II pressure sensors is 0.4 mb (Brock et al. 1986).

The pressure gradient term was computed from a two-pass Barnes objective analysis (Barnes 1964; Koch et al. 1983) of the reduced PAM-II and hourly surface-station pressures on a 30×17 grid covering the southern Plains. The grid spacing was approximately 33 km in both the zonal and meridional directions. For an advective speed of 5 m s^{-1}, which was determined from the wind data, space can be converted to time so that for a convergence parameter γ of 0.5, the amplitude of disturbances having periods shorter than 3 h was mostly eliminated (as it was in the temporally filtered PAM-II wind data). For the average station separation of 100 km, the Barnes filter parameter k was 19 000 km^2 (9500 km^2) on the first (second) pass. The radius of influence ($k^{0.5}$) was therefore approximately 140 km (100 km) on the first (second) pass. The pressure at each PAM site was then estimated through bilinear interpolation of the gridded data. Finally, the pressure gradient was computed by fitting a plane to the pressures at each PAM-II site in each triangle.

The density used in the calculation of the acceleration due to the pressure gradient force (1) was estimated using linear interpolation to the centroids of each triangle of the density, computed using the ideal gas law, at each PAM-II site in the triangle.

Bell and Bosart (1988), in a study of Appalachian cold-air damming based on conventional surface data, calculated the sum of the turbulent mixing terms ($\mathbf{F}_H + \mathbf{F}_Z = \mathbf{F}_H + \mathbf{F}_D + \mathbf{F}_A$) in (1) as a residual. Colle and Mass (1995) used the same technique in a study of cold surges east of the Rocky Mountains. In our study, since we have time series of the horizontal wind components at 1-min intervals, we can calculate the horizontal mixing term explicitly and estimate $\mathbf{F}_Z$ as a residual. The vertical mixing term $\mathbf{F}_A$ can be estimated if the surface drag is computed using (5). The vertical mixing term $\mathbf{F}_A$ is thought to be of fundamental importance to the dynamics of the dryline (e.g., Schaefer 1974b) and has never, to the best of our knowledge, been estimated near the dryline from real data.

The correlations in the horizontal-mixing term [$\mathbf{F}_H$ in (2)] were computed using a 6-h time average centered on the time of the analysis (using 360 wind observations). From (2) and (3), we find that for $|u'| \sim |v'| \sim |w'| \sim 1$ m s^{-1}, $|\mathbf{F}_H| \ll |\mathbf{F}_Z|$ when the horizontal scale is on the order of 100 km and the vertical scale is on the order of 1 km.

Because the vertical-mixing term $\mathbf{F}_Z$ itself, from which $\mathbf{F}_A$ is computed, is calculated as a residual, $\mathbf{F}_A$

represents both the actual physical effects of vertical mixing *and* the combined effects of errors accumulated in the calculations of the other terms. We must therefore be very careful in interpreting the results of our analyses. Since the calculation of $\mathbf{F}_D$ requires an estimate of the drag coefficient C_D (dimensionless), which introduces further uncertainty into our estimate of $\mathbf{F}_A$, the degree of error associated with the *quantitative* estimates of $\mathbf{F}_A$ requires that we can make only *qualitative* estimates about the behavior.

For a typical drag coefficient on the order of 10^{-3} (Stull 1988, 267; C_D over the Plains varies from 1.3×10^{-3} to 1.5×10^{-3} at night and to 1.8×10^{-3} during the day) and wind speed at anemometer level of 10 m s^{-1}, the surface drag is on the order of 1×10^{-4} m s^{-2} [cf. (5)]. Parameterizing $\mathbf{F}_A$ as

$$\mathbf{F}_A = \frac{1}{1000 \text{ m}}\left(-K\frac{\partial|\mathbf{v}|}{\partial z}\frac{\mathbf{v}}{|\mathbf{v}|}\right) \tag{8}$$

with a typical value of K of 1 m^2 s^{-1} (Stull 1988, 206), we note that $\mathbf{F}_A$ is only on the order of $[(1 \text{ m}^2 \text{ s}^{-1})(10 \text{ m s}^{-1})(10^3 \text{ m})^{-1}]$ $(1000 \text{ m})^{-1} = 1 \times 10^{-5}$ m s^{-2}, which is an order of magnitude smaller than surface drag. However, since K may be up to two orders of magnitude larger in a highly convective regime (Wyngaard 1982, 75), we expect that $\mathbf{F}_A$ might be as important as surface drag in the well-mixed boundary layer near the dryline during the daytime. For example, turbulent fluctuations in u and w (i.e., u' and w') in dry convection near the ground are on the order of 1–5 m s^{-1} (Stull 1988, 444, 461). If u increases with height, then convective mixing should bring low u up ($u' < 0$ and $w' > 0$) and high u down ($u' > 0$ and $w' < 0$). In a 1000-m-deep convective boundary layer in which there is vigorous mixing,

$$-\frac{\partial\overline{u'w'}}{\partial z} \approx \frac{(1 \text{ m s}^{-1})(1 \text{ m s}^{-1})}{1000 \text{ m}} \approx 0.001 \text{ m s}^{-2},$$

which is an order of magnitude larger than the acceleration induced by surface drag. However, the estimate above is probably a bit high since u' and w' are multiplied together, and they are often smaller than 1 m s^{-1}. Evidence that the boundary layer near the dryline during COPS-91 was in fact highly convective is seen in Crawford and Bluestein (1997), in which plots of virtual temperature as a function of time at PAM sites are shown that exhibit rapid (10-min scale and less), high-amplitude (1–1.5 K) fluctuations, characteristic of a convective boundary layer.

4. Near-dryline dynamics

The mesoscale dynamics near the dryline are discussed in terms of hourly force diagrams (or acceleration diagrams) at the surface both east and west of the dryline for two cases during COPS-91. Since the retrieval of the vertical-mixing term as a function of the other terms in the equation of motion (1) is most accurate if there is a linear variation of both the horizontal wind components and the pressure among the three neighboring PAM-II mesonet sites, we excluded times during which the location of the dryline or the pressure trough lay within the triangles formed by the three neighboring sites. There were a number of cases in which triangles of PAM-II sites lay just to the east of the dryline, especially in the eastern Texas panhandle and western Oklahoma. However, in all but one of these cases the pressure trough passed through the PAM-II triangle during the afternoon. There were relatively few cases in which triangles of PAM-II sites lay to the west of the dryline and trough. Furthermore, during some of the cases in which the triangles lay to the west of the dryline and trough, data from one of the PAM-II sites were missing. During COPS-91 the dryline seemed to be situated relatively far west most of the time in comparison to its position during other years, when it had progressed into western Oklahoma. Thus, we can only present one time series of force diagrams east of the dryline and two time series west of the dryline.

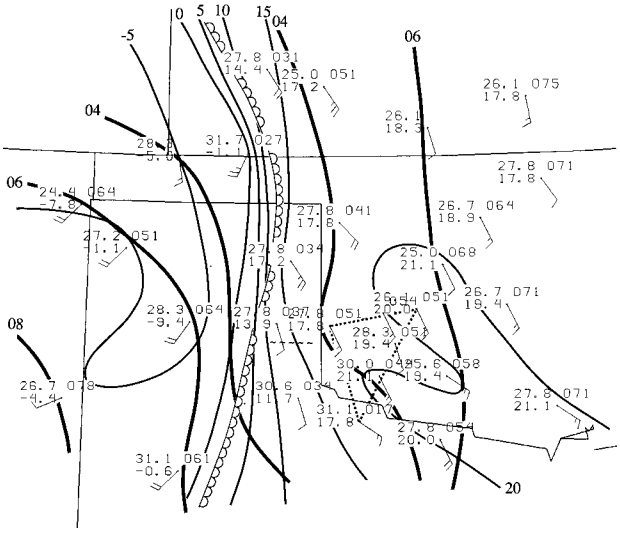

FIG. 2. Surface map for the COPS-91 region of western Oklahoma, the Texas panhandle, and adjacent areas at 2300 UTC 15 May 1991. Location of the dryline is denoted by the scalloped line. Temperature (upper left) and dewpoint (lower left) are plotted in degrees Celsius; altimeter setting in millibars times 10, without the leading "10," is plotted to the right [the altimeter setting plotted at Chillicothe (cf. Fig. 1) is approximately 1.5 mb too low]; half (whole) wind barb represents 2.5 (5) m s^{-1}. Triangle of Erick–Chillicothe–Corn PAM-II sites is highlighted by dotted lines. A portion of the flight leg of the NOAA P-3 from which wind data were used to retrieve the pressure gradient is indicated by a line of tilde marks.

a. Force diagram east of the dryline

On 15–16 May (Fig. 2), when there were severe convective storms east of the dryline later on during the early evening, the local time derivative and advection terms (and horizontal mixing) are relatively small (Fig.

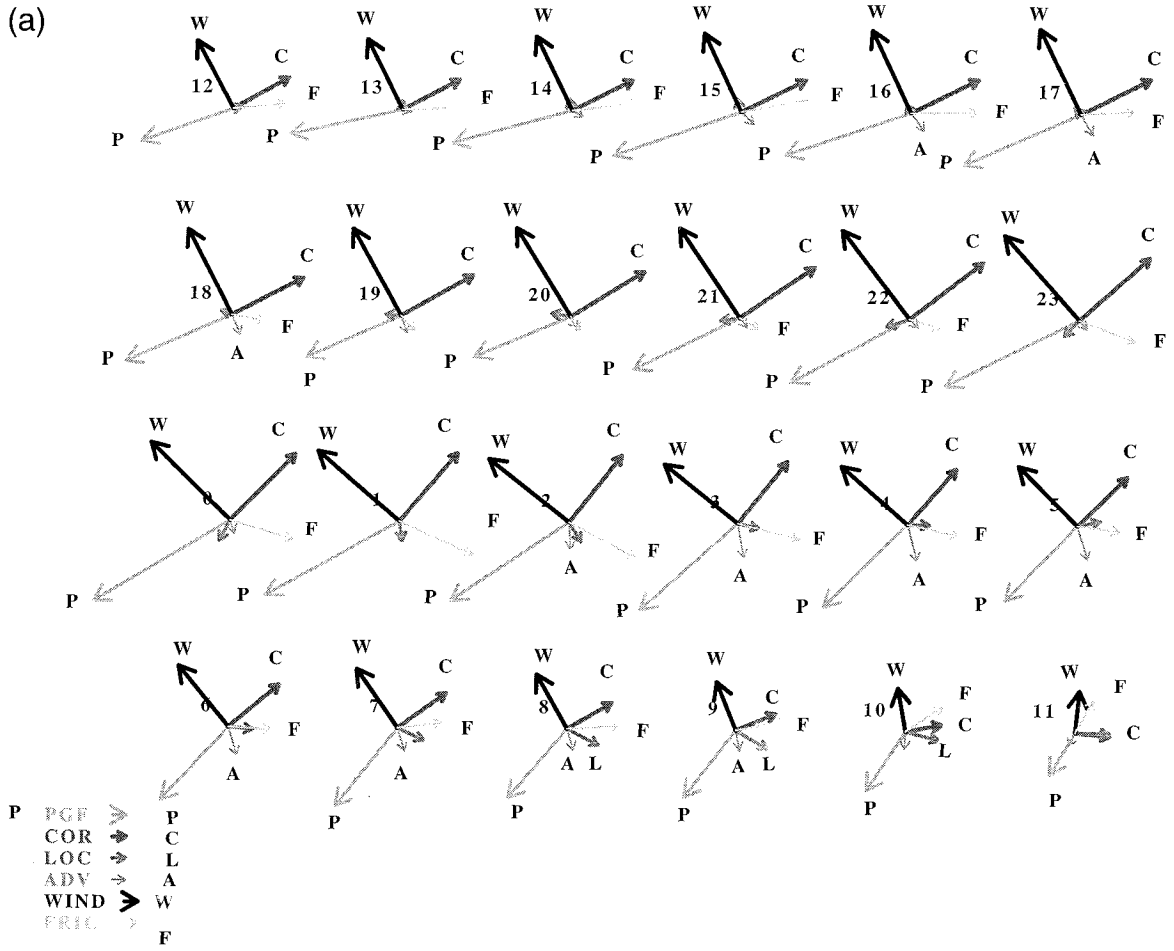

FIG. 3. (a) Force diagrams east of the dryline at hourly intervals at the centroid of the triangle formed by the locations of the Erick–Chillicothe–Corn PAM-II mesonet sites (Fig. 2) on 15–16 May 1991; time in UTC shown to left of wind vector in each force diagram. LOC(**L**), ADV(**A**), COF(**C**), PGF(**P**), and FRIC(**F**) solid vectors represent the local acceleration ($\partial\mathbf{v}/\partial t$), advective acceleration [$(\mathbf{v}\cdot\nabla)\mathbf{v}$], acceleration due to the Coriolis force ($-f\mathbf{k}\times\mathbf{v}$), acceleration due to the pressure gradient force [$-(1/\rho)\nabla p$], and acceleration due to the friction force ($\mathbf{F}_Z$) [cf. Eq. (1)]. Each acceleration that is negligibly small in comparison to the largest terms is not labeled (in this figure, $\mathbf{F}_H$ does not appear at any time). Wind vector **v** is depicted by WIND(**W**); the scale of **v** is not the same as the scale of the forces because the units are different. (b) Zonal (x-) component of the accelerations due to the forces, and the zonal component of the wind as a function of time. Positive (negative) values denote components directed toward the east (west).

3a). The wind remains from the southeast most of the day, and the friction term is directed opposite and to the right of the wind. This is similar to what Brown (1991, 447, Fig. 11.14) and Arya (1985) have found for a balanced, barotropic boundary layer. The pressure gradient is relatively large and has a substantial component directed across the dryline (cf. Fig. 2). The force diagram for 15–16 May therefore looks like the classic

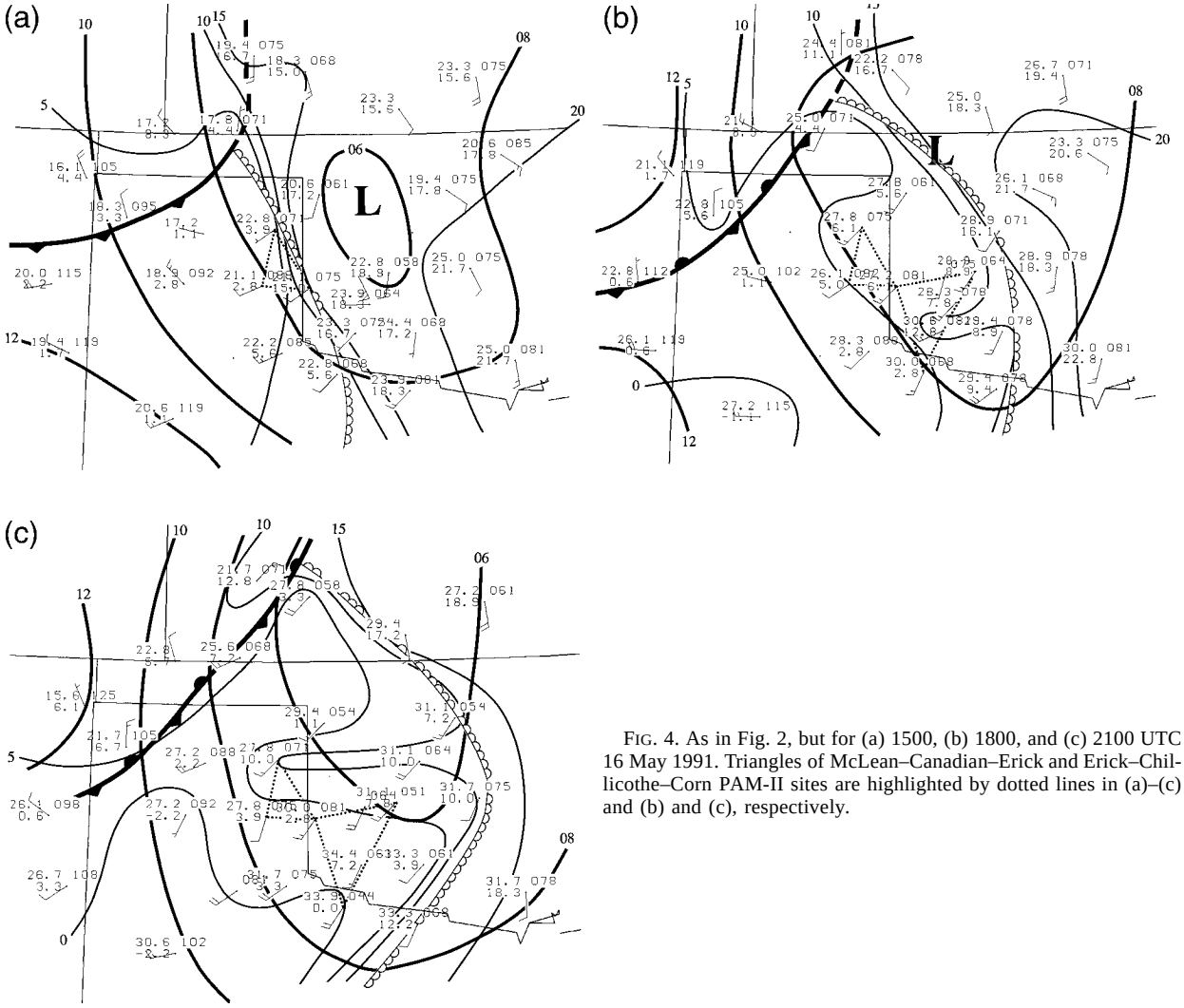

FIG. 4. As in Fig. 2, but for (a) 1500, (b) 1800, and (c) 2100 UTC 16 May 1991. Triangles of McLean–Canadian–Erick and Erick–Chillicothe–Corn PAM-II sites are highlighted by dotted lines in (a)–(c) and (b) and (c), respectively.

balance-of-forces diagram for a barotropic Ekman layer (Arya 1985).

The cross-dryline component of the pressure gradient has a maximum easterly component an hour before the cross-dryline component of the wind has a maximum easterly component (Fig. 3b). The pressure gradient force is the largest force, while the Coriolis and friction forces are smaller.

b. Force diagrams west of the dryline

Only two series of force diagrams valid west of the dryline and the pressure trough could be calculated. On 16 May the dryline passed through western Oklahoma (Fig. 4). Early in the day the dryline was located west of a surface low pressure area/pressure trough; the dryline propagated eastward and caught up to the low/trough during the afternoon in central Oklahoma, where it displayed a prominent ''bulge.'' The forces west of the dryline during only the late morning through late afternoon could be calculated (Figs. 5 and 6). The winds remain veered around to the southwest direction. The friction term is oriented mainly in the direction opposite and to the *left* of the wind (Fig. 5a) in the McLean–Canadian–Erick triangle. Since the advective term is comparable in magnitude to the other terms, the flow is relatively unbalanced. In an area east of that valid in Fig. 5a, the friction term is also directed opposite and to the *left* of the wind (Fig. 6a). However, in the latter area the flow is relatively balanced.

The cross-dryline component of the wind undergoes a well-defined oscillation, with a maximum in westerly component around 1900–2100 UTC (Figs. 5b, 6b). We disregard in Fig. 5b (Fig. 6b) terms before 1500 (1700) UTC or after 2300 (2100) UTC, when the dryline was either in or west of the triangle of PAM-II mesonet stations whose data were used in the force calculations. The magnitude of the cross-dryline component (west to east) of the pressure gradient term slowly increased throughout the day and appeared to have no correlation

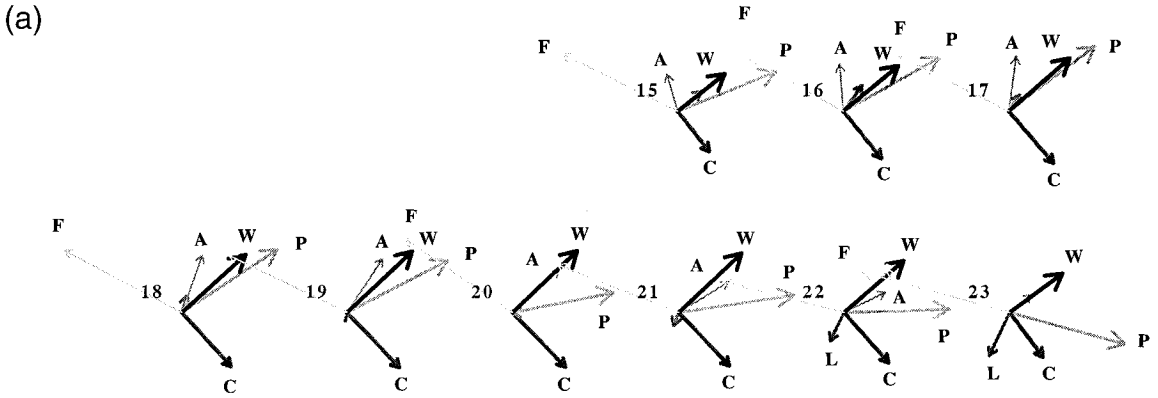

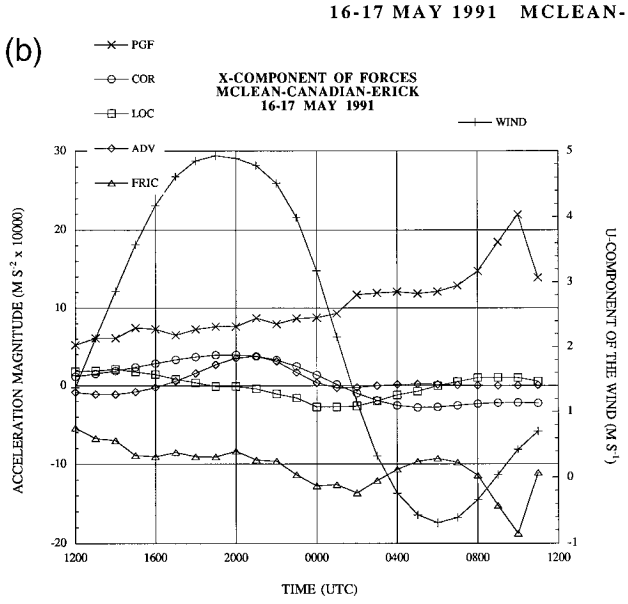

FIG. 5. As in Fig. 3, but west of the dryline at the centroid of the triangle formed by the locations of the McLean–Canadian–Erick PAM-II mesonet sites (Fig. 4) on 16 May 1991. The dryline was either in or west of the triangle before 1500 and after 2300 UTC.

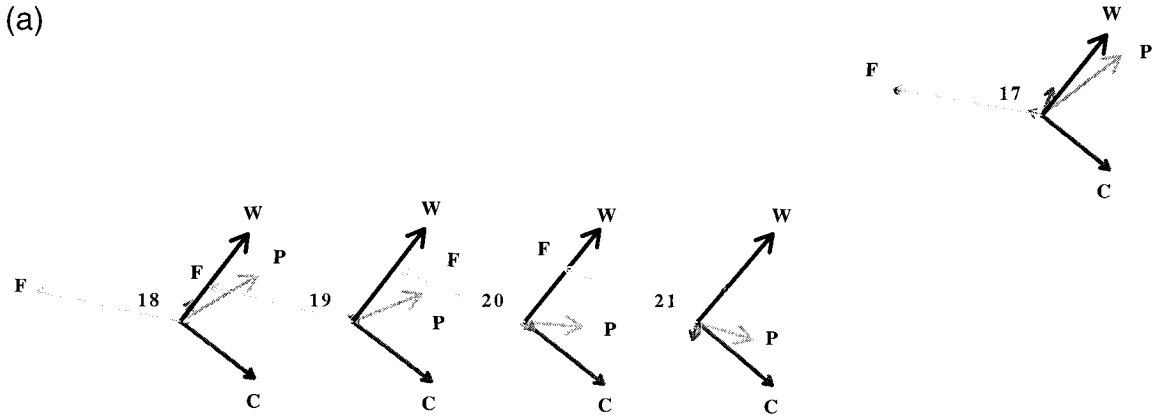

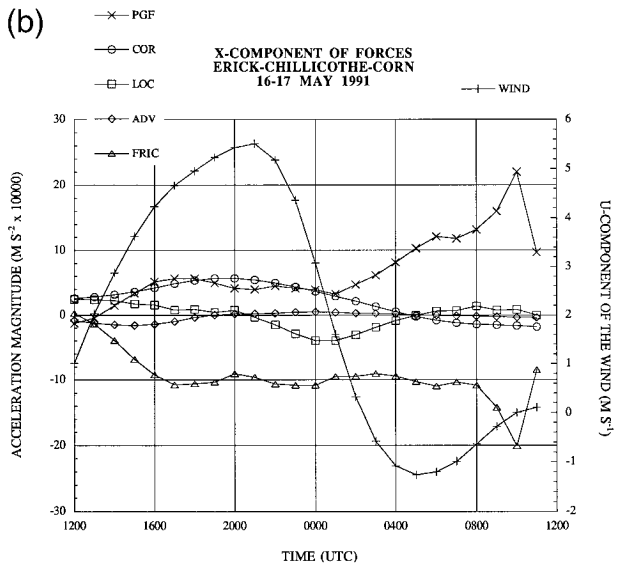

FIG. 6. As in Fig. 3, but west of the dryline at the centroid of the triangle formed by the locations of the Erick–Chillicothe–Corn PAM-II mesonet sites (Figs. 4b and 4c) on 16 May 1991. The dryline was either in or west of the triangle before 1700 and after 2100 UTC.

with the cross-dryline component of the wind (Fig. 5b) in the McLean–Canadian–Erick triangle. The cross-dryline component of the friction term also slowly increased. The other terms were much smaller than the friction and pressure gradient terms (Fig. 5b). In the Erick–Chillicothe–Corn triangle the pressure gradient term also appeared to have no correlation with the cross-dryline component of the wind (Fig. 6b). In this case, the pressure gradient term was relatively small during the day.

c. *Sensitivity of the retrieval to the pressure gradient term*

The force diagrams discussed in the previous sections must be interpreted with caution because the vertical mixing term was computed as a residual. The first and second terms in (1) are on the order of

$$\frac{\partial|\mathbf{v}|}{\partial t} \approx \frac{1 \text{ m s}^{-1}}{1 \text{ h}} \approx 10^{-4} \text{ m s}^{-2}$$

$$|\mathbf{v}||\nabla\mathbf{v}| \approx \frac{(10 \text{ m s}^{-1})(1 \text{ m s}^{-1})}{100 \text{ km}} \approx 10^{-4} \text{ m s}^{-2}.$$

The upslope–downslope component at the surface ($\mathbf{v}\cdot\nabla z$, where z is the elevation of the surface) is at most (5 m s^{-1}) (1 km/1000 km) = 0.5 cm s^{-1} (cf. Figs. 3b, 5b, and 6b for observed values of u). Then the third term in (1) is at most

$$|w|\left|\frac{\partial\mathbf{v}}{\partial z}\right| \approx \frac{(0.5 \text{ cm s}^{-1})(10 \text{ m s}^{-1})}{1 \text{ km}} = 5 \times 10^{-5} \text{ m s}^{-2}.$$

Since the magnitudes of the local time derivative and advective terms were an order of magnitude less than the Coriolis and pressure gradient terms [first and second terms, respectively, on the right-hand side of (1)], which were on the order of 10^{-3} m s^{-2}, the first and second terms were not a significant source of error. The neglect of the vertical-advection-of-momentum term in (1) ($w\partial\mathbf{v}/\partial z$) was justified because the zonal component of the surface wind was generally less than 5 m s^{-1} and hence $|w\partial\mathbf{v}/\partial z|$ was much less than the Coriolis and pressure gradient terms. East of the dryline the Coriolis term was less than the pressure gradient term for the 15–16 May case, as was found by Bell and Bosart (1988) in their cold-air damming case. Since the pressure gradient term was sometimes the largest term in the equation of motion, and its value is somewhat uncertain owing to (i) instrument error, (ii) the process of reduction to a mean elevation, (iii) the mixture of temporally filtered mesonet pressure data and temporally filtered hourly altimeter setting data, and (iv) the objective analysis of all the pressure data, we must therefore consider the sensitivity of the retrieved friction term to errors in the pressure gradient.

The rms error of the pressure data (σ) used in the calculation of the horizontal pressure gradient is

$$\sigma = (\sigma_{\text{ins}}^2 + \sigma_{\text{red}}^2)^{0.5}, \tag{9}$$

where σ_{ins} and σ_{red} are the rms errors in pressure due to instrument inaccuracy and reduction of pressure to the mean elevation, respectively, and it is assumed that the former and latter are statistically independent; errors in the reduction of pressure to the mean elevation are due to errors in temperature and errors in elevation. The elevation of each station was derived from topographic maps, not from a Global Positioning System (GPS). The rms error due to the pressure reduction, σ_{red}, was estimated to be 0.1 mb by reducing the pressures in the triangles using standard atmosphere and dry-adiabatic lapse rates and comparing the reduced pressures using each lapse rate and by considering possible errors in station elevation that were not corrected for; the lapse rate near the ground was assumed to lie in between the standard-atmosphere rate and the dry-adiabatic rate. This procedure is best justified during the daytime, in the absence of a strong surface-based inversion. The value of σ_{ins} is approximately 0.4 mb (Brock et al. 1986); σ is therefore approximately 0.4 mb.

The rms error of the magnitude of the pressure gradient, σ_{PG}, which is based upon pressure observations made at the vertices of a right triangle, one of whose sides is oriented in the east–west direction and one of whose sides is oriented in the north–south direction, is as follows (Thiebaux and Pedder 1987, 43–44):

$$\sigma_{\text{PG}} = \frac{\sigma}{(A \sin\alpha)^{0.5}}, \tag{10}$$

where A is the area of the triangle and α is the angle the hypotenuse makes with the east–west direction. For simplicity we consider an isosceles triangle, for which α is 45°. The triangles used in this study were neither exactly right nor exactly isosceles, and hence the estimate in (10) is subject to uncertainty. For stations separated by 100 km, the rms error in pressure gradient is 5.7×10^{-7} kPa m^{-1}, and the rms error in the acceleration due to the pressure gradient force is 5.7×10^{-4} m s^{-2}. The actual pressure gradients are on the order of 1 mb (100 km)$^{-1}$, which corresponds to an acceleration of approximately 10^{-3} m s^{-2}. However, the objective analysis procedure, which filters 95% of the pressure variations on timescales shorter than 3 h, effectively reduces the variance of the pressure measurements at each station, so the rms errors in the acceleration due to the pressure gradient force are less than the 50%–60% as suggested for unsmoothed pressure data. Furthermore, since the actual estimated pressure gradients were often around two to three times greater, the rms error in acceleration due to the pressure gradient force is around 20%–30% or less.

As an independent check of the accuracy of the pressure gradient estimates, we used perturbation-pressure analyses computed from retrievals based upon wind data (furnished by C. Hane) collected during the P-3 aircraft's stepped-traverse patterns across and approxi-

mately normal to the dryline (Hane et al. 1993). The technique used to retrieve the pressure field is detailed in Hane and Ray (1985). Turbulent friction was parameterized using the method described in Smagorinsky (1963). As in Parsons et al. (1991), we neglected variations along the dryline (i.e., in the north–south direction). On 15 May (cf. Fig. 2) the center of the P-3 flight track was located about 100 km west and 20 km north of the centroid of the Erick–Chillicothe–Corn triangle, where the surface pressure gradient was computed from the PAM-II data. The retrieved east–west pressure gradient at low levels (the pressure gradient did not vary significantly with height in the boundary layer) east of the dryline at 2330 UTC was -2.1 mb (100 km)$^{-1}$, which is compared with the east–west component of the surface pressure gradient of -1.2 mb (100 km)$^{-1}$ calculated at the centroid of the triangle for the average of the 2300 and 0000 UTC data. The retrieved pressure gradients were not computed for the identical locations for which the surface triangle computations were done, and the retrievals neglected along-the-dryline variations in wind and employed a parameterized form of friction; although the difference in pressure gradient estimates agreed in sign, the pressure gradient magnitudes computed for several triangle calculations (for the Erick–Chillicothe–Corn and McLean–Canadian–Erick triangles) differed by 40%–75% of each other.

The pressure gradient vector from the force diagram in Fig. 3a was therefore perturbed by vectors whose magnitudes are 25% and 50% of the magnitude of the pressure gradient vectors and whose directions are along, opposite, normal and to the right, and normal and to the left of the pressure gradient vectors. The friction acceleration was then retrieved for the four ''perturbed'' pressure gradients. It was found (not shown) that the friction acceleration due to vertical mixing ($\mathbf{F}_Z$) was directed opposite and to the right of the wind for the case shown in Fig. 3a for all perturbations except the one in which the pressure gradient was perturbed to the right by 50%; in this case the retrieved frictional acceleration was relatively small. Friction $\mathbf{F}_Z$ was directed opposite and to the left of the wind for *all* (of the aforementioned) perturbations for the case shown in Fig. 5a. We therefore have confidence in the qualitative aspects of our findings. However, when all forces and the wind are relatively weak, small perturbations in the pressure gradient can result in qualitatively different retrieved friction vectors. We therefore disregard or interpret with extreme caution the retrieved friction term when the pressure gradient is weak, as sometimes happens during the late night and early morning hours. During these times the boundary layer may become decoupled from the flow aloft owing to a radiation inversion.

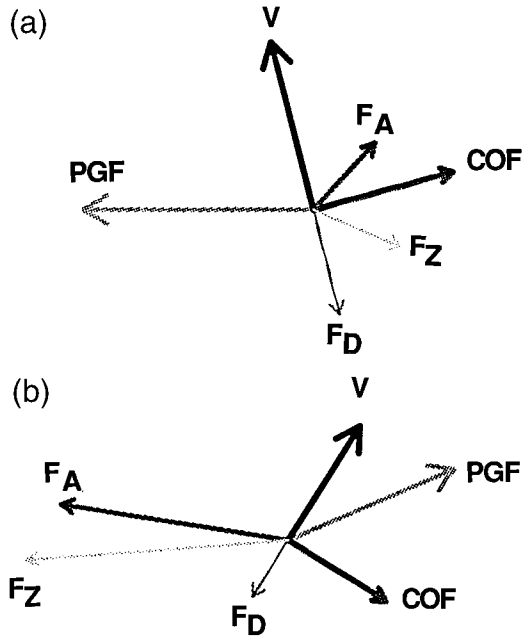

FIG. 7. Generalization of the forces and their relationships to the wind (**V**, not drawn to the same scale as the friction forces because the units are different) during the day (a) east of the dryline when the pressure gradient force is strong compared to the Coriolis force and pointing in nearly the opposite direction and (b) west of the dryline. It is assumed that the flow is balanced, that is, that the sum of the local and advective derivatives of the wind is negligible. PGF and COF represent the pressure gradient and Coriolis forces, respectively. Term $\mathbf{F}_Z$ represents the total force due to the turbulent vertical mixing of horizontal momentum, where $\mathbf{F}_Z = \mathbf{F}_D + \mathbf{F}_A$; $\mathbf{F}_D$ represents the vertical mixing of horizontal momentum at anemometer level with the stationary ground below (drag); and $\mathbf{F}_A$ represents the vertical mixing of horizontal momentum at anemometer level with the air above. A drag coefficient of 1.5×10^{-3} was used to compute $\mathbf{F}_D$.

5. Summary and conclusions

A new method for estimating the forces at anemometer level has been developed and applied to datasets from an intensive field experiment in the southern Plains when the dryline was present. The success of the method suggests that mesonetworks can yield information that can be used to explain the dynamical nature of some boundary layer phenomena.

East of the dryline during the late morning and afternoon when a strong pressure trough was located near the dryline, *the vertical-mixing term in the equation of motion acted in the opposite direction and to the right of the wind* (Fig. 3a), as is expected in a barotropic Ekman layer (Fig. 7a). This finding is valid even if the estimate of the pressure gradient is in error by as much as 25%–50% in magnitude.

Since the surface drag $\mathbf{F}_D$ acts in the direction opposite that of the wind (5), it follows from (4), by solving for $\mathbf{F}_A$, that vertical mixing from above has the effect of accelerating the flow normal and to the right of the wind. This is consistent with an environment near anemometer level in which the wind veers with height (and the wind speed does not vary substantially) and horizontal momentum from aloft is mixed downward but the layer in which the mixing occurs is not well mixed. It is also consistent with a wind profile near

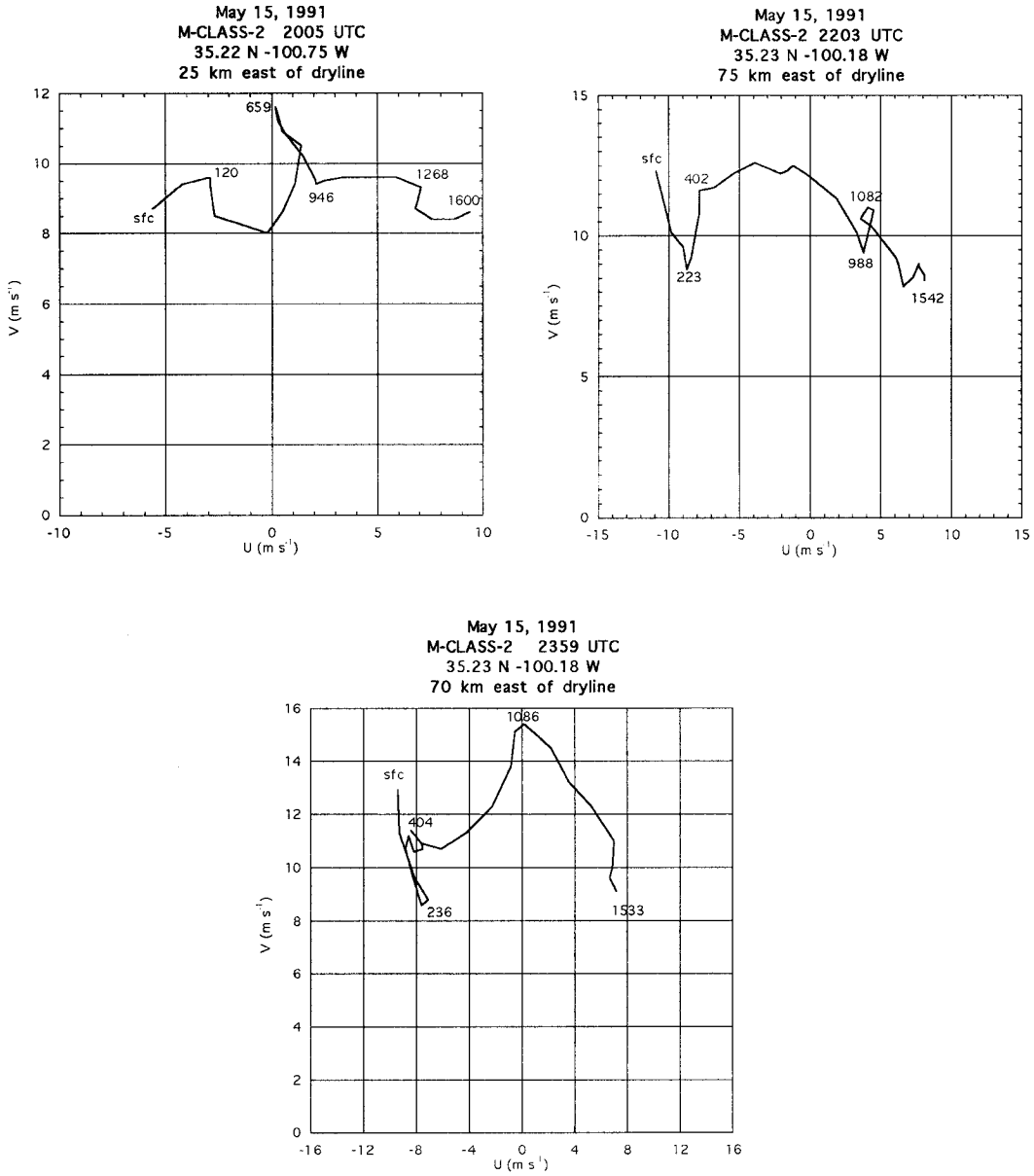

FIG. 8. Hodographs derived from mobile CLASS soundings released within 100 km east of the dryline on 15 May 1991. The heights in meters AGL are indicated.

anemometer level in which the second derivative of the component of wind normal to the wind at anemometer level is positive, that is, in which the component of wind normal and to the right of the wind at anemometer level increases slowly with height and then more rapidly. Hodographs derived from mobile CLASS soundings released east of the dryline on 15 May 1991 (Fig. 8) show a general clockwise turning from a few hundred meters to a kilometer or so above the ground. This clockwise turning with height is consistent with classic Ekman layer behavior. Below several hundred meters, however, the hodograph curves in the opposite direction in two of the three hodographs displayed, mostly because the wind speed decreases above the surface and then increases above a few hundred meters; the latter behavior, however, may be suspect.

West of the dryline, when a pressure trough is located to the east, *the vertical-mixing term in the equation of motion acted to the left of the wind* (Figs. 5a and 6a). This finding is valid even if the estimate of the pressure gradient is in error by as much 25%–50% in magnitude. In this case the surface winds are highly ageostrophic and the wind is directed nearly perpendicular to the isobars. Such a relationship (Fig. 7b) is unlike that found in a barotropic Ekman layer. Bannon and Salem (1995) showed how the effect of a linear variation in geo-

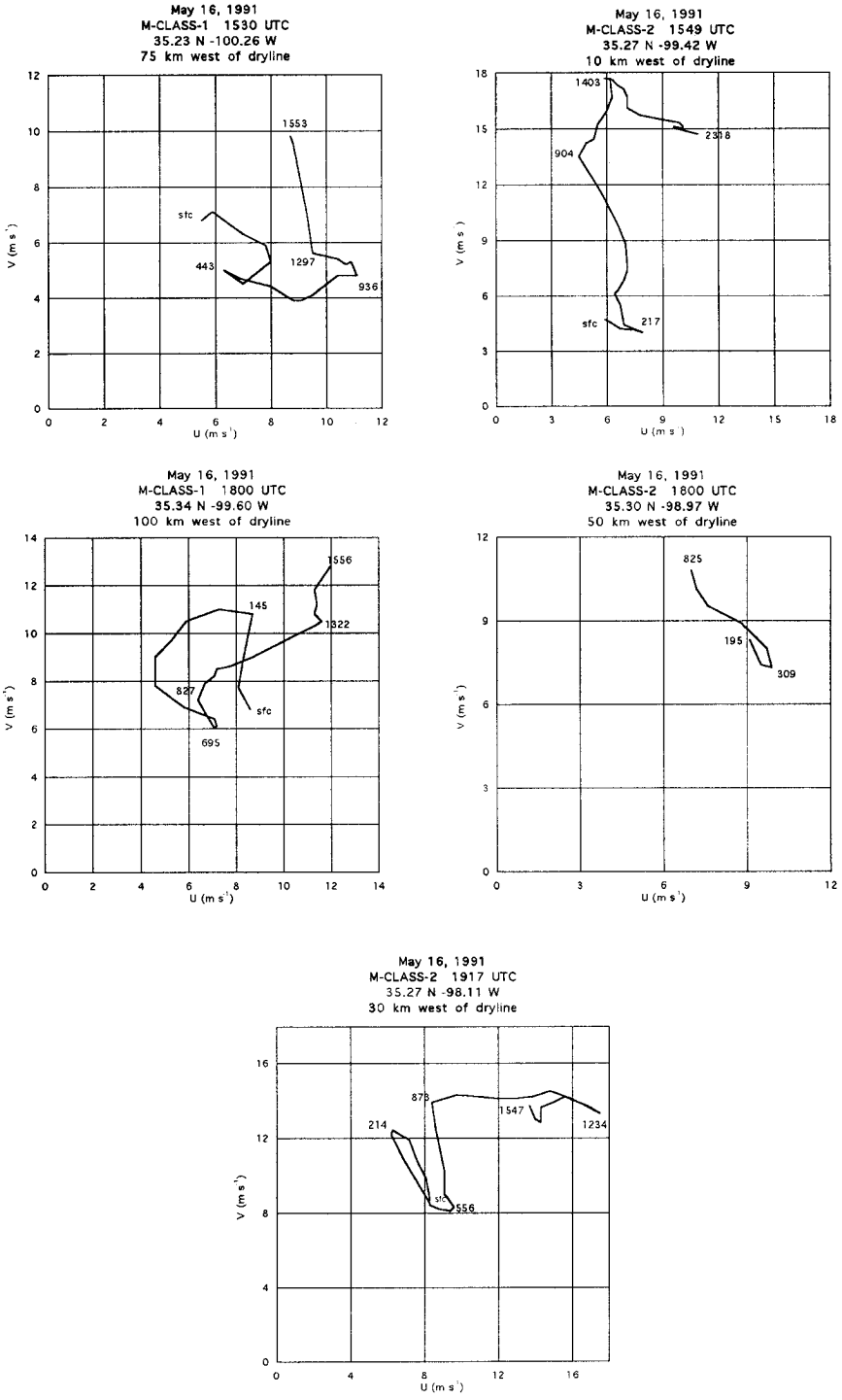

FIG. 9. As in Fig. 8, but for mobile CLASS soundings released within 100 km west of the dryline on 16 May 1991.

strophic wind with height due to a horizontal temperature gradient is a surface flow that has an added component both along and normal to the gradient. If a warm-core pressure trough is superimposed over a poleward-directed temperature gradient, then west of the trough there must be an ageostrophic component of the wind that turns the wind from westerly to west-southwesterly or southwesterly. In other words, there is cold advection west of the pressure trough, which must be associated with a backing of the wind with height. In

the deep mixed layer west of the dryline, the more southerly momentum is probably mixed down to anemometer level and results in a backing of the surface wind. Hodographs derived from mobile CLASS soundings released west of the dryline on 16 May 1991 (Fig. 9) generally exhibit counterclockwise turning with height below a kilometer or so above the ground and backing of the winds with height at low levels. We therefore believe that the component of friction acting unexpectedly to the left of the wind is due to baroclinic effects.

A maximum easterly (i.e., cross-dryline, from the moist side toward the dry side) component to the wind during the evening hours usually lags a maximum in horizontal pressure gradient, which is directed westward (again, from the moist side toward the dry side), by a few hours. These observations are in accord with the inland sea-breeze hypothesis (Sun and Ogura 1979; Sun and Wu 1992) and the modeling study of Ziegler et al. (1995). In model simulations ''wind blowing from the cool side to the warm side [an offshore (i.e., from east to west) air flow]'' is generated as ''the horizontal pressure gradient pointing toward the negative x direction (i.e., toward the west) is intensified'' (Sun and Ogura 1979).

The computation of the pressure gradient and the gradients of the wind components was complicated by the sloping terrain. It might be possible to improve the analysis of surface forces by working in a terrain-following coordinate system. However, the physical interpretation of each term would be more complicated. Gal-Chen and Somerville (1975) showed how with an irregular lower boundary an extra term involving the vertical derivative of pressure is added to the horizontal pressure gradient. In our calculations we implicitly take into account this extra term when we reduce hydrostatically the station pressures to a common elevation. Since the pressure gradient term is usually much larger than the advective term, the calculation of the former is more of a problem.

This study made use of a modest network of mesonet sites. Since COPS-91 was conducted, a denser, *operational* network of over 100 mesonet stations has been installed in Oklahoma (Brock et al. 1995). With this network, higher resolution (in both space and time) studies are possible. Efforts are currently underway to use the analysis techniques described herein to study the dryline when it passes into the new network; the results are forthcoming.

Acknowledgments. This study was funded by NSF research Grants ATM-9019821 and ATM-9302379. The Surface and Sounding Systems Facility of ATD at NCAR provided the PAM-II stations. The PAM-II stations received partial support from the National Aeronautics and Space Administration through Steve Koch. Some of this research was done while the first author was a summer visitor at the MMM Division of NCAR. The NCAR Graphics group assisted with most of the figures. NCAR is funded by the National Science Foundation. Sue Weygandt at OU/CAPS also assisted with some of the figures. We are indebted to personnel at NSSL for providing the M-CLASS soundings and the PAM-II site surveys. Irv Watson (NSSL) provided some data not available in the OU archive. Carl Hane (NSSL) assisted with the pressure retrievals. Fred Carr (OU), Bob Davies-Jones (NSSL), Carl Hane (NSSL), Conrad Ziegler (NSSL), John Brown (FSL), and Mark Morrissey (OU) provided helpful advice. Jeanne Schneider, Zbigniew Sorbjan, and Doug Lilly (OU) are acknowledged for their turbulent discussions about mixing.

REFERENCES

Arya, S. P. S., 1985: The schematics of balance of forces in the planetary boundary layer. *J. Climate Appl. Meteor.,* **24,** 1001–1002.

Bannon, P. R., and T. L. Salem Jr., 1995: Aspects of the baroclinic boundary layer. *J. Atmos. Sci.,* **52,** 574–596.

Barnes, S. L., 1964: A technique for maximizing details in numerical weather map analysis. *J. Appl. Meteor.,* **3,** 396–409.

Bell, G. D., and L. F. Bosart, 1988: Appalachian cold air damming. *Mon. Wea. Rev.,* **116,** 137–161.

Bluestein, H. B., 1992: *Synoptic–Dynamic Meteorology in Midlatitudes.* Vol. I, *Principles of Kinematics and Dynamics.* Oxford University Press, 431 pp.

Brock, F. V., G. H. Saum, and S. R. Semmer, 1986: Portable Automated Mesonet II. *J. Atmos. Oceanic Technol.,* **3,** 573–582.

——, K. C. Crawford, R. L. Elliot, G. W. Cuperus, S. J. Stadler, H. L. Johnson, and M. D. Eilts, 1995: The Oklahoma mesonet: A technical overview. *J. Atmos. Oceanic Technol.,* **12,** 5–19.

Brown, R. A., 1991: *Fluid Mechanics of the Atmosphere.* Academic Press, 489 pp.

Colle, A. B., and C. F. Mass, 1995: The structure and evolution of cold surges east of the Rocky Mountains. *Mon. Wea. Rev.,* **123,** 2577–2610.

Crawford, T. M., and H. B. Bluestein, 1997: Characteristics of dryline passage during COPS-91. *Mon. Wea. Rev.,* **125,** 463–477.

Davies-Jones, R., 1993: Useful formulas for computing divergence, vorticity, and their errors from three or more stations. *Mon. Wea. Rev.,* **121,** 713–725.

Fujita, T. T., and R. M. Wakimoto, 1982: Effects of miso- and mesoscale obstructions on PAM winds obtained during Project NIMROD. *J. Appl. Meteor.,* **21,** 840–858.

Gal-Chen, T., and R. C. J. Somerville, 1975: Numerical solution of the Navier–Stokes equations with topography. *J. Comput. Phys.,* **17,** 276–310.

Hane, C. E., and P. S. Ray, 1985: Pressure and buoyancy fields derived from Doppler radar data in a tornadic thunderstorm. *J. Atmos. Sci.,* **42,** 18–35.

——, C. L. Ziegler, and H. B. Bluestein, 1993: Investigation of the dryline and convective storms initiated along the dryline: Field experiments during COPS-91. *Bull. Amer. Meteor. Soc.,* **74,** 2133–2145.

——, H. B. Bluestein, T. M. Crawford, M. E. Baldwin, and R. M. Rabin, 1997: Severe thunderstorm development in relation to along-dryline variability: A case study. *Mon. Wea. Rev.,* **125,** 231–251.

Koch, S. E., and J. McCarthy, 1982: The evolution of an Oklahoma dryline. Part 2: Boundary-layer forcing of mesoconvective systems. *J. Atmos. Sci.,* **39,** 237–257.

——, M. desJardins, and P. J. Kocin, 1983: An interactive Barnes objective map analysis scheme for use with satellite and conventional data. *J. Climate Appl. Meteor.,* **22,** 1487–1503.

McCarthy, J., and S. E. Koch, 1982: The evolution of an Oklahoma dryline. Part I: Meso- and subsynoptic-scale analysis. *J. Atmos. Sci.,* **39,** 225–236.

Ogura, Y., and Y. Chen, 1977: A life history of an intense mesoscale convective storm in Oklahoma. *J. Atmos. Sci.,* **34,** 1458–1476.

Parsons, D. B., M. A. Shapiro, R. M. Hardesty, R. J. Zamora, and J. M. Intrieri, 1991: The finescale structure of a west Texas dryline. *Mon. Wea. Rev.,* **119,** 1283–1292.

Rhea, J. O., 1966: A study of thunderstorm formation along dry lines. *J. Appl. Meteor.,* **5,** 58–63.

Rust, W. D., D. W. Burgess, R. A. Maddox, L. Showell, T. Marshall, and D. Lauritzen, 1990: Testing a mobile version of a Cross-Chain LORAN Atmospheric (M-CLASS) Sounding System. *Bull. Amer. Meteor. Soc.,* **71,** 173–180.

Schaefer, J. T., 1973: On the computation of the surface divergence field. *J. Appl. Meteor.,* **12,** 546–547.

——, 1974a: The life cycle of the dryline. *J. Appl. Meteor.*, **13,** 444–449.

——, 1974b: A simulative model of dryline motion. *J. Atmos. Sci.*, **31,** 956–964.

Smagorinsky, J., 1963: General circulation experiments with the primitive equations. I. The basic experiment. *Mon. Wea. Rev.*, **91,** 99–164.

Stull, R. B., 1988: *An Introduction to Boundary Layer Meteorology.* Kluwer, 666 pp.

Sun, W.-Y., and Y. Ogura, 1979: Boundary layer forcing as a possible trigger to squall line formation. *J. Atmos. Sci.*, **36,** 235–254.

——, and C.-C. Wu, 1992: Formation and diurnal variation of the dryline. *J. Atmos. Sci.*, **49,** 1606–1619.

Thiebaux, H. J., and M. A. Pedder, 1987: *Spatial Objective Analysis.* Academic Press, 43–45.

Wyngaard, J. C., 1982: Boundary-layer modeling. *Atmospheric Turbulence and Air Pollution Modelling,* F. T. M. Nieuwstadt and H. van Dop, Eds., D. Riedel, 69–106.

——, 1984: The mean wind structure of the baroclinic, convective boundary layer. *Proc. First Sino-American Workshop on Mountain Meteorology,* Beijing, China, Science Press and Amer. Meteor. Soc., 371–395.

Ziegler, C. L., W. J. Martin, R. A. Pielke, and R. L. Walko, 1995: A modeling study of the dryline. *J. Atmos. Sci.*, **52,** 263–285.